JOURNAL OF MATERIALS SCIENCE: MATERIALS IN MEDICINE, 5 (1994) 147–153

Plasma-sprayed hydroxyapatite coating: effect of different calcium phosphate ceramics

D. M. LIU, H. M. CHOU, J. D. WU
Materials Research Laboratories, Industrial Technology Research Institute, Hsinchu, Chutung, 31015, Taiwan

Three kinds of calcium phosphate ceramic powders, namely commercial hydroxyapatite (CHA), self-made hydroxyapatite (SMHA) and synthesized hydroxyapatite (SHA), are employed as starting materials for plasma-sprayed coating onto a stainless steel (316L) substrate. Results show a mixture of hydroxyapatite (HA), tricalcium phosphate (TCP), and tetracalcium phosphate (TeCP) phases appearing in the CHA and SHA-derived coatings and a primary of a HA with trace contents of tricalcium phosphate phases resulting in the SMHA-derived coating. The HA appears to be the only observable crystalline phase present in the SMHA-derived coating after 7 days of incubation with a simulated body fluid (SBF); however, part of the impurities, i.e. TCP and TeCP, remain in the other coatings. No apparent microcracks can be found on the coated surfaces when SMHA and SHA are used. The poor packing density of SHA reflects its weakness in bonding strength to the substrate surface compared with that obtained using CHA and SMHA powders. The surface morphology of the coatings was found to alter significantly after a sufficient period of incubation.

1. Introduction

It is well-known that plasma-sprayed coatings of hydroxyapatite (HA) have the ability to induce new bone ingrowth and subsequently increase fixation stability [1–5]. Much clinical evidence has indicated that the presence of HA can promote osseteointegration between bone and implant devices [6]. Although several reports [7, 8] indicated that HA coating may degrade fail either on the interface or on the surface, work involved in the development of a satisfactory HA coating has received worldwide attention.

Accordingly, a satisfactory HA coating must be dense, adherent, and with structures not altered irreversibly by the coating techniques [8]; 95% crystalline HA phase is required [9, 10]. To meet these requirements, plasma-sprayed-induced phase decomposition [11] and phase transformation [12, 13] must be avoided by using large starting particles, varying plasma-sprayed atmospheres, and controlling plasma spraying parameters to optimize the particle melting and flow conditions [14]. To maintain the crystal structure of HA, several attempts at improving plasma-sprayed coatings have been tried, for instance, by employing pure inert gas plasma, such as argon gas or Ar/He gas plasma, instead of a typical Ar/H_2 plasma [8, 14]. This is because the inert gases are chemically inert and thermally low in enthalpy, which makes HA more stable than when adding H_2.

Although the above-mentioned plasma-sprayed coatings do show attractive features, their relatively low interfacial strength, poor packing density and expensive pure Ar or He gas render this application commercially impractical. Therefore, to enhance the interfacial strength, a high-temperature plasma was used by incorporating hydrogen gas in Ar; however, HA undergoes decomposition [11].

In this study, three kinds of calcium phosphate ceramic powders, namely commercial hydroxyapatite (CHA), self-made hydroxyapatite (SMHA), and synthesized hydroxyapatite (SHA), were employed as starting materials for plasma-sprayed coating onto a stainless steel (316L) substrate. Attempts at assessing the parameters for optimizing the coating and controlling the factors that may decrease the efficacy of bioactivity are discussed.

2. Experimental procedures

2.1. Powder morphology and plasma spraying condition

Three kinds of powder were employed, namely CHA, SMHA, and SHA. The CHA powder (Amdry 6021, Alloy Metals Inc.) has a size of 45–165 μm and an irregular particle shape, Fig. 1. The SMHA, which was synthesized using a gel method [15], has a size of 5–35 μm and spherical in shape, Fig. 2. The SHA, which is made at the Paffenbarger Research Center at the American Dental Association (ADA), has a particle size of about 8–40 μm and mostly are near-spherical in appearance, Fig. 3. The powders were sprayed onto a sand-blasted stainless steel (316) plate with dimensions 2.0×5.0 cm. The plasma sprayer (Plasma Technik AG, System 3000S-CDS) was operated at atmospheric pressure at 450 A, 69 V, with a working distance of 10–12 cm. A mixture of Ar/H_2 gas at flow rates of 10 l/min and 40 l/min was used as carrier gas.

0957–4530

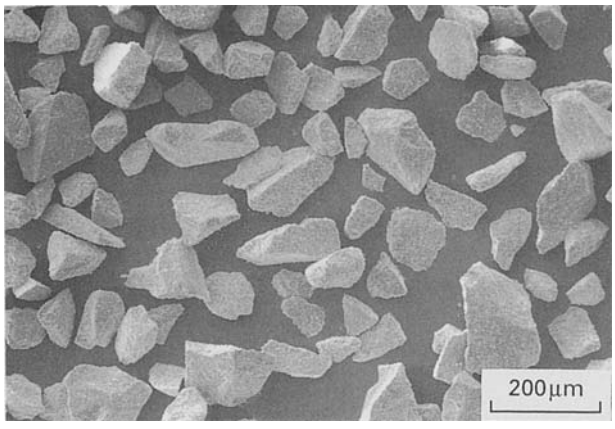

Figure 1 Commercially available hydroxyapatite powder (CHA).

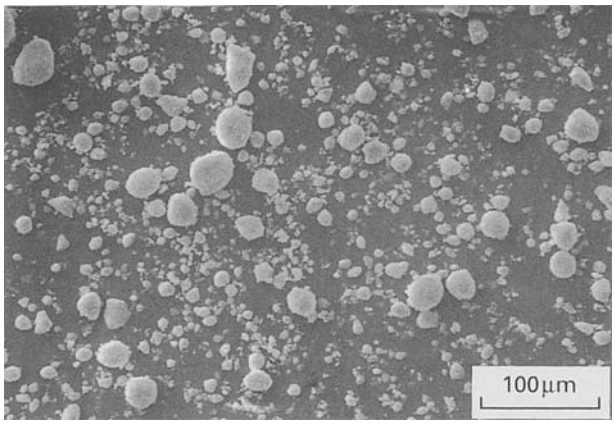

Figure 2 Hydroxyapatite powder synthesized in this laboratory (SMHA).

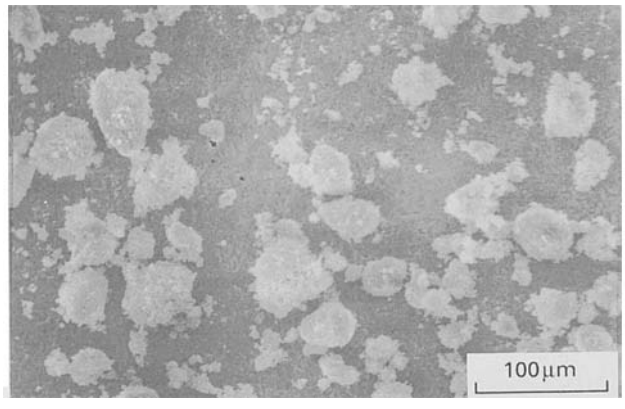

Figure 3 Hydroxyapatite powder provided from Paffenbarger Research Center, American Dental Association (SHA).

2.2. Characterization

The resulting coatings were examined using X-ray diffraction (Philips, PW 1700) with a CuK_α radiation and a scanning speed of 0.01°/s for crystalline phase analysis. The X-ray diffractometer was equipped with a computerized diffractogram analyser. The microstructure and surface morphology of the coatings, and the interface between coating and substrate were investigated by scanning electron microscopy (SEM, Cambridge Instruments, S-360). Bonding strength between the coatings and substrate was determined using an Instron tester (Model 1361).

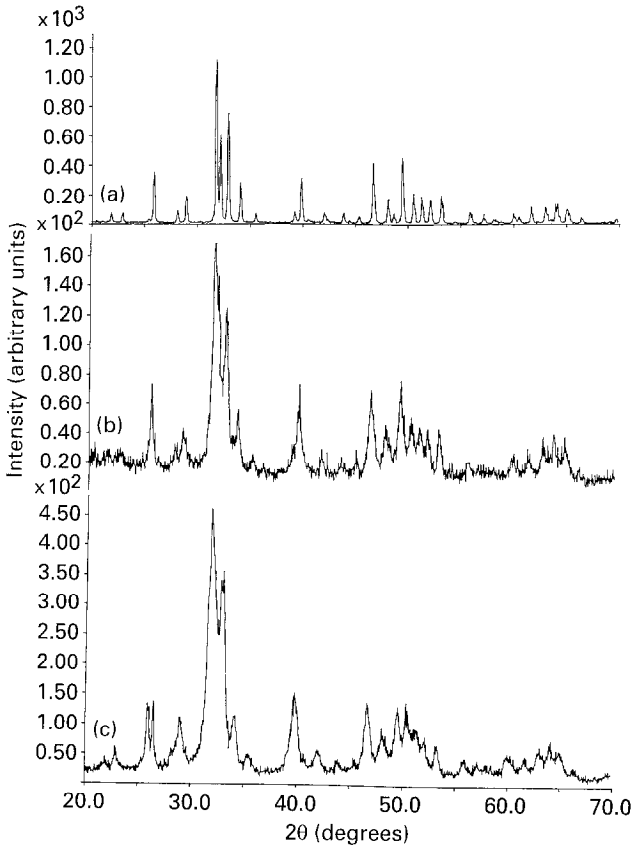

Figure 4 X-ray diffraction analysis of the starting (a) CHA, (b) SMHA, and (c) SHA powders.

An *in-vitro* experiment was conducted by immersing the coated substrates into a simulated body fluid (referred to as SBF), which has almost the same ion concentration as that in human blood plasma, for 7 days at 38 °C. The as-immersed coatings were then characterized.

3. Results and discussion

3.1. Characteristics of the starting powders

The molar ratios of Ca/P for the starting CHA, SMHA, and SHA powders were 1.66, 1.68, and 1.60, respectively, as determined by means of an inductively coupled plasma-atomic emissive spectrometer (ICP-AES). Fig. 4 shows the X-ray diffraction patterns of these powders: whereas the CHA is a highly crystalline material (Fig. 4a), the SMHA appears to have the poorest crystalline (Fig. 4b), i.e. it may be constructed by a short-range-order apatitic structure, according to their relative diffraction intensity based on the same diffraction parameters.

Fig. 5a to 5c illustrate the infrared analyses of the starting CHA, SMHA, and SHA powders, respectively. Infrared analysis is used because it usually reveals material characteristics which cannot be differentiated by means of X-ray diffraction. Most of the peaks are attributed to two kinds of vibrations [16]; three PO_4^{3-} stretching vibration modes at 960, 1040, and 1080 cm^{-1} and two PO_4^{3-} bending modes at 570 and 600 cm^{-1}. The OH^- stretching mode at around 3570 cm^{-1}, where the SMHA powder (Fig. 5b) shows

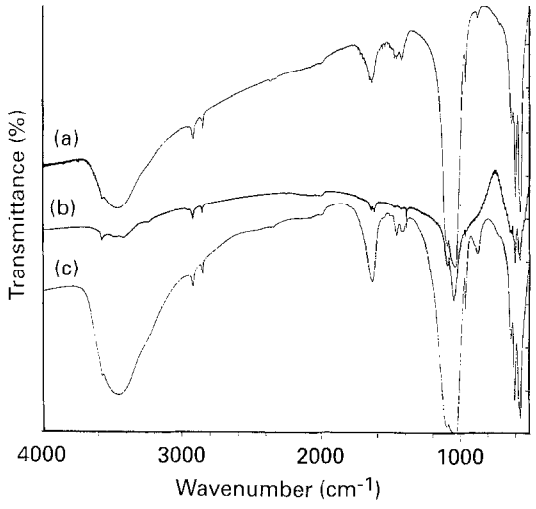

Figure 5 Fourier transformed infrared analysis of the starting (a) CHA, (b) SMHA, and (c) SHA powders.

a relative-sharp absorption peak (compared to the other two powders), and a flexural mode at 630 cm^{-1} were clearly observed. Additionally, a certain amount of CO_3^{2-} ion was observed in each spectrum at 1400 and 872 cm^{-1}, where the latter absorption band is barely visible in the SMHA powder (Fig. 5b). These findings indicate that sufficient amounts of CO_3^{2-} ion are present in the starting CHA and SHA apatite structures, but are of low content only, in the SMHA powder.

3.2. X-ray diffraction analysis of the coatings

X-ray diffraction patterns of the plasma-sprayed coatings revealed that the crystalline phases are primarily a mixture of HA, α-TCP and TeCP for plasma-sprayed CHA and SHA, Fig. 6a and c, respectively. The former coating consists of crystalline HA phase with a small amount of impurities, nevertheless, a sufficient amount of impurities exist in the latter one. A mixture of HA with trace contents of tetracalcium phosphate ($Ca_4P_2O_9$) was observed for the plasma-sprayed SMHA, Fig. 6b. The formation of $Ca_4P_2O_9$ and/or α-$Ca_3(PO_4)_2$ phases is apparently due to phase decomposition of the starting powders during plasma spraying according to the reaction [11, 17]:

$$Ca_{10}(PO_4)_6(OH)_2 \Leftrightarrow 2Ca_3(PO_4)_2 + Ca_4P_2O_9 + H_2O \quad (1)$$

In fact, the α-TCP and TeCP existing in the plasma-sprayed CHA and SMHA coatings are only in small amounts compared to those in the SHA coating. One possible reason is directly related to their starting stoichiometric Ca/P ratios [11].

The plasma-sprayed SMHA coating appeared to provide, from the crystallographic viewpoint, a more satisfactory coating than the others [9, 10]. However, the actual reason why the SMHA powder yields an almost single HA coating, in contrast to the coatings generated from the others is not well understood. More complete melting of the SMHA powder during plasma spraying may have contributed, although

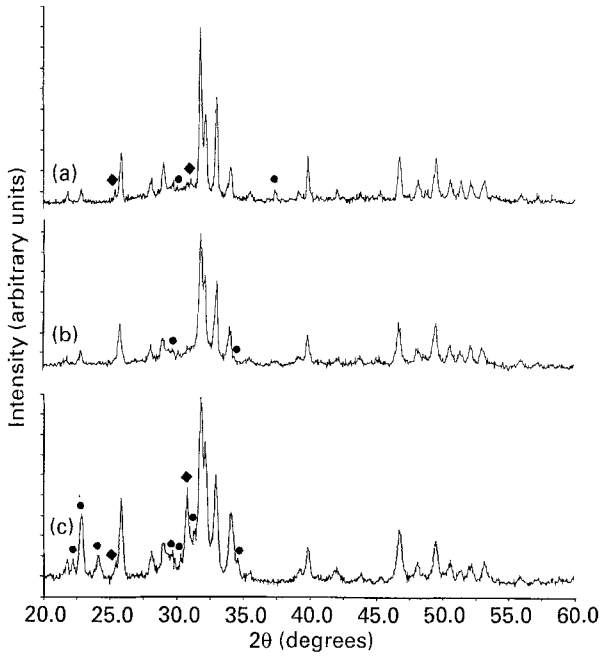

Figure 6 X-ray diffraction patterns of the plasma-sprayed (a) CHA, (b) SMHA, and (c) SHA coatings (● TCP; ◆ TeCP).

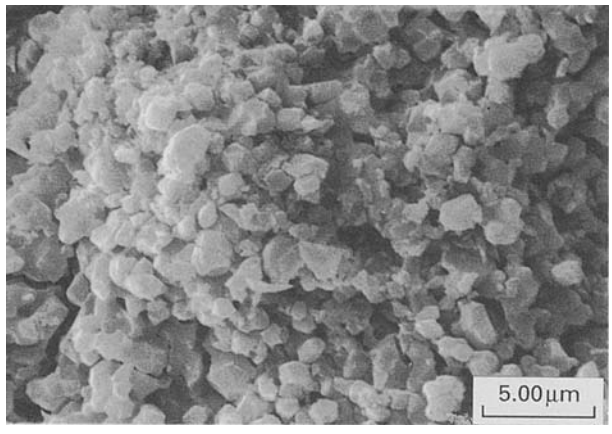

Figure 7 Large magnification of the plasma-sprayed CHA coating showing fine particles which were not melted during spraying.

Wolke *et al.* [18] believed complete melting of the particles would result in an amorphous coating. However, after impinging against the substrate (having a surface temperature about 150 °C), the HA crystals, having a short-range-order of apatitic arrangement, precipitate immediately during solidification. For the CHA coating, its highly crystalline HA phase (Fig. 6a) may partly be attributed to the small grains within the aggregated particles, which are not yet melted (Fig. 7) during spraying, and result in a mostly crystalline HA coating; however, small contents of α-TCP and TeCP result.

The SMHA powder, which has the poorest crystallinity, may have a similar degree of melting to that of the SHA powder due to the similarity in powder morphology and particle size [11]. However, the SHA powder produced an unsatisfactory coating; the large deviation from stoichiometric Ca/P ratio of 1.67 may principally be responsible. Accordingly, this suggests that the stoichiometric Ca/P ratio and crystallinity of the starting calcium phosphate ceramic powders play

a key role in determining the crystallographic structure of the resulting HA coating, which may subsequently affect biodegradation behaviour *in-vivo* [19, 20].

Upon soaking in a simulated body fluid, which has almost the same ion concentration as that of human blood plasma, for 7 days, the crystal structure of the CHA and SHA coatings changed significantly, but only little variation occurred in the SMHA coating, as revealed by X-ray diffraction analysis, Fig. 8a to 8c. The characteristic peaks of HA in the CHA coating became broader and weaker in relative diffraction intensity compared with Fig. 4a; however, they became more pronounced in the SHA coating. The $Ca_4P_2O_9$ phase in both coatings disappeared and the α-TCP was also reduced. According to Skinner *et al.* [21] and Newesely [22], the $Ca_4P_2O_9$ and α-TCP undergo transformation by

$$3Ca_4P_2O_9 + H_2O \rightarrow HA + 2Ca^{2+} + 4OH^- \quad (2)$$

and

$$4Ca_3(PO_4)_2 + 3H_2O \rightarrow HA + 2Ca^{2+} + 2HPO_4^{2-} \quad (3)$$

The existence of the residual TCP phase, in Fig. 8(a) and (c), suggests that reaction (3) takes place, but is less active than reaction (2), and the increase in calcium concentration accompanied by a decrease in phosphorus in the simulated fluid, listed in Table I, substantiates reaction (2). The reason for the reduction in phosphorus is not well understood, although several reports has shown an increase of phosphorus in the SBF for long-period immersion [11, 18]; an apatite deposition by reaction between the calcium and phosphate ions (may be provided from the surrounding body fluid) in the close vicinity of the surface may be a plausible explanation [23, 24].

However, there is no large change in crystal structure for the SMHA coating (Fig. 8b), although considerable change in ion concentration has been observed and this could be due to the occurrence of reaction (3) (since TCP is the only impurity) together with other unknown surface reaction(s). However, these findings indicate that the starting SMHA powder provides a stable HA coating *in vitro*.

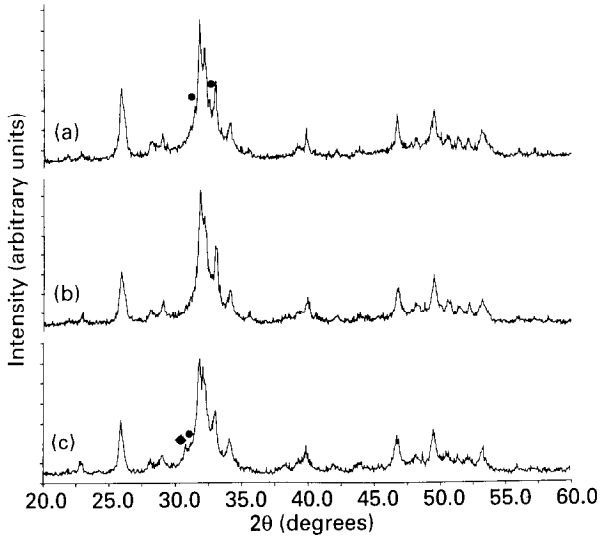

Figure 8 X-ray diffraction patterns of the plasma-sprayed (a) CHA, (b) SMHA, and (c) SHA coatings after 7 days of immersion in simulated body fluid (● TCP; ◆ TeCP).

TABLE I. Variation of calcium and phosphate ion concentration before and after 7 days of immersion in simulated body fluid (SBF)

Materials	Ca (ppm)	P (ppm)
Original SBF	83	37.5
CHA coating	110	24.4
SMHA coating	102	20.5
SHA coating	85.4	27.7

3.3. Microstructure analysis

The coating surfaces, Fig. 9a to c, are relatively dense

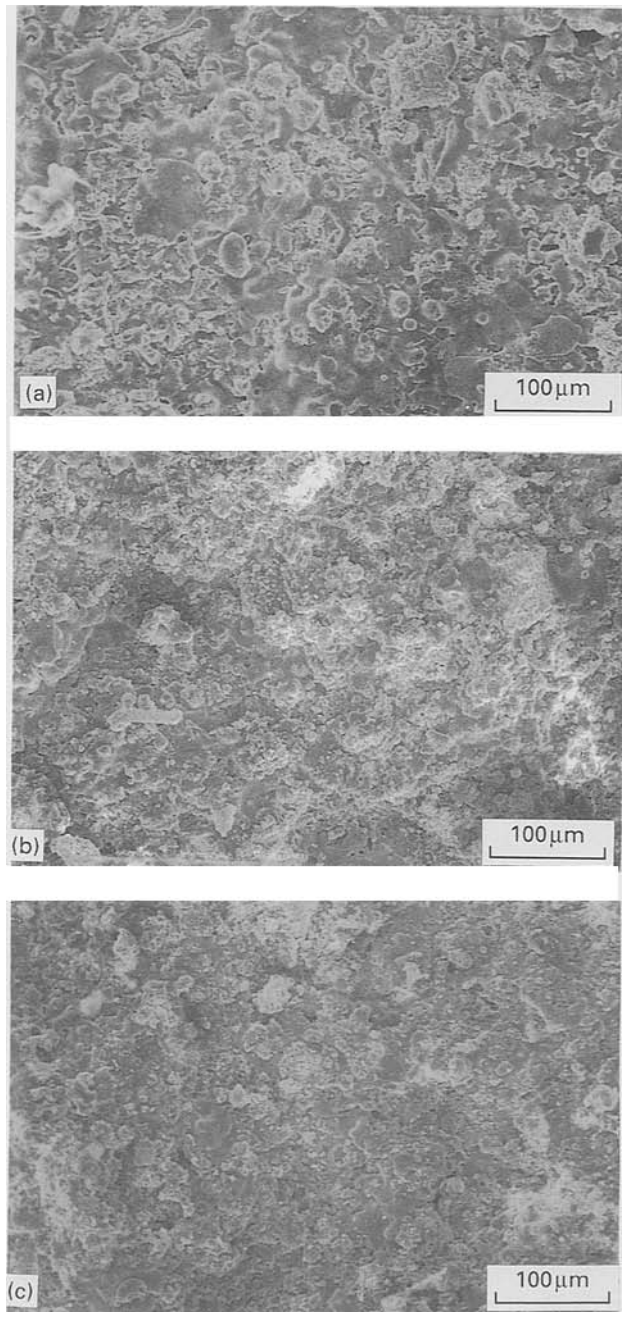

Figure 9 Surface morphology of the plasma-sprayed (a) CHA, (b) SMHA, and (c) SHA coatings.

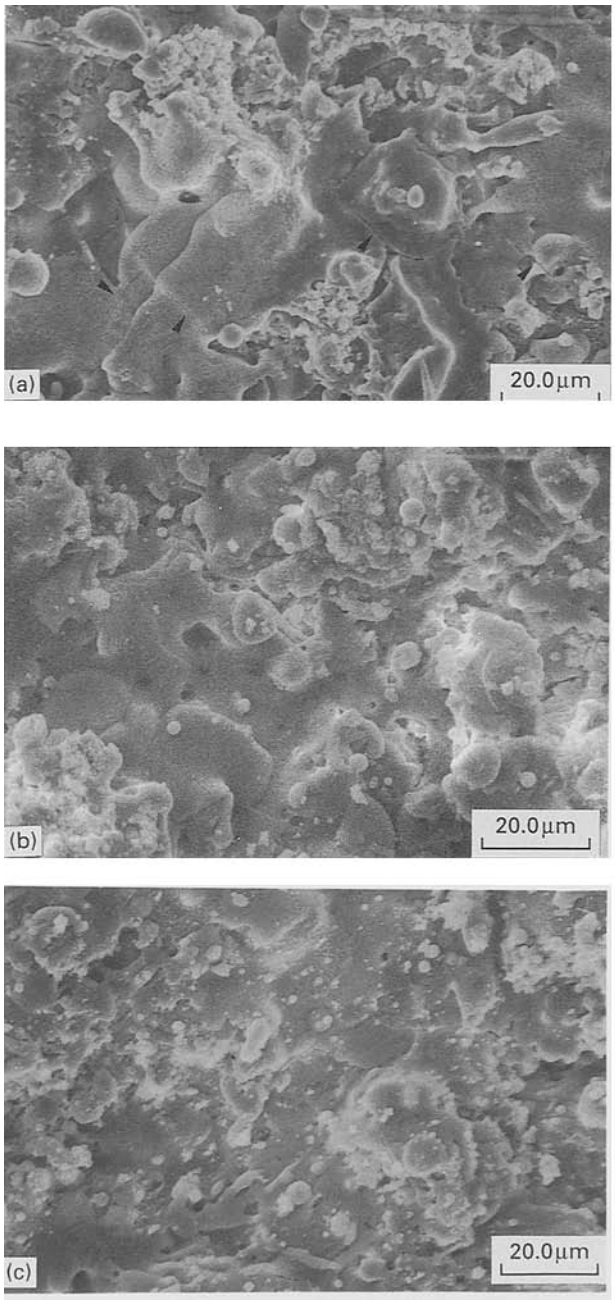

Figure 10 Large magnification of Fig. 9 for the plasma-sprayed (a) CHA, (b) SMHA, and (c) SHA coatings.

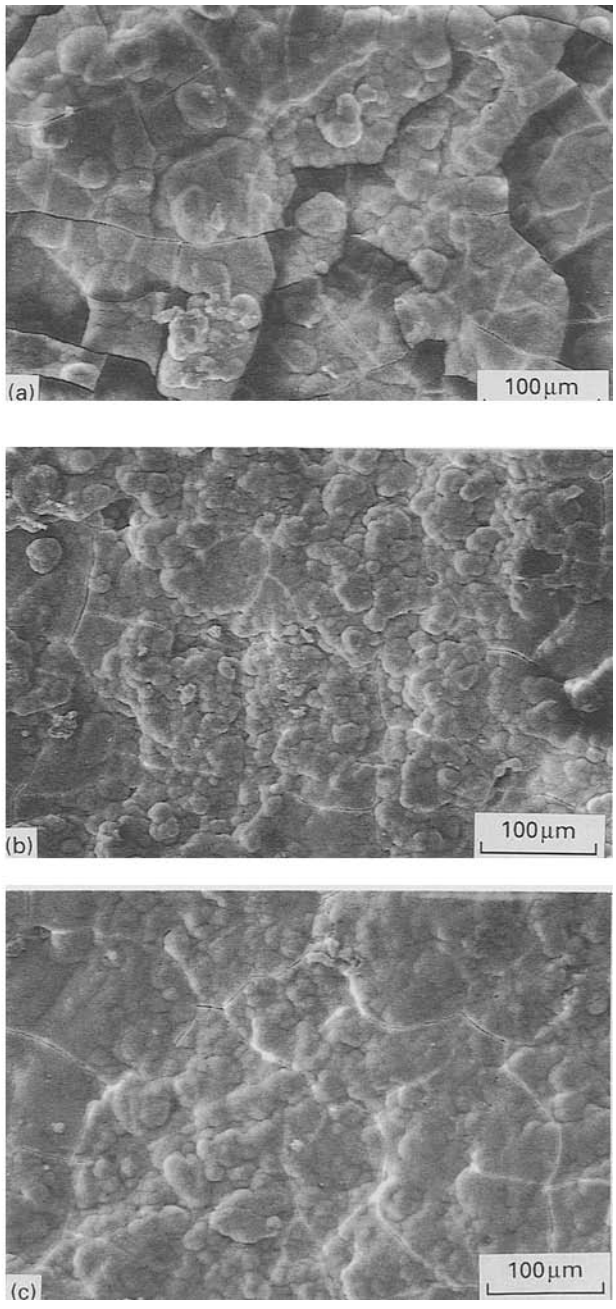

Figure 11 Surface morphology of the plasma-sprayed (a) CHA, (b) SMHA, and (c) SHA coatings after 7 days of immersion in the simulated body fluid at 38 °C.

and homogeneous in appearance. There seems to be more coarser particles in the surface of the CHA coating than in the SMHA and SHA coatings, which may result from easier melting of the SMHA and SHA powders than CHA in the plasma stream. However, at a high magnification, the coated surfaces are non-homogeneous, Fig. 10a to c, since they consist of a large area of glassy surface with many randomly distributed sphere-like particles and micropores. In fact, plasma spraying usually causes cracks on the coating surface, as observed in CHA coating (Fig. 9a). This mainly results from the thermal expansion mismatch between the substrate and calcium phosphate ceramic, together with the residual stresses induced from cooling. However, these cracks could lead to local stress concentration and give rise to further mechanical and physico-chemical instability of the coatings [11]. Fortunately, no observable cracks can be found in the surface when using SMHA and SHA powders (Fig. 9b and c). This phenomenon may be postulated by assuming that when well-molten calcium phosphate ceramic powders impinge against the metal surface, it is still viscous at the very beginning of cooling, and subsequently reduces the internal stresses by accommodating interfacial thermal expansion mismatch, so that cracks are avoided.

After 7 days of incubation with SBF, a significant difference in surface morphology of the coatings, Fig. 11a to c, compared with those before immersion, Fig. 9a to c, can be clearly observed, i.e. numerous cracks and ball-like grains appeared on the surface. The occurrence of these cracks and ball-like materials is believed to result from diffusion and reaction between the coating surface and the SBF, e.g. reactions (2) and (3). In fact, at large magnification, Fig. 12a to c

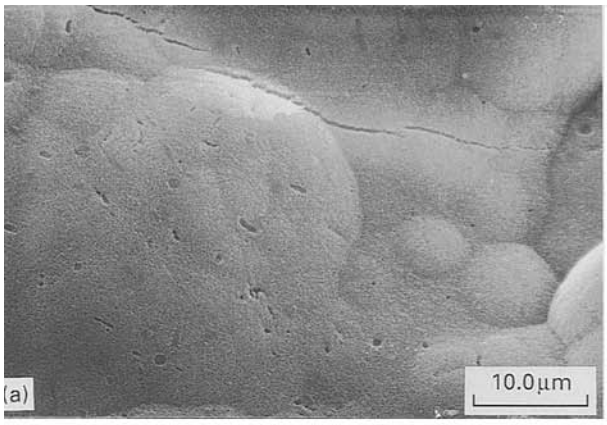

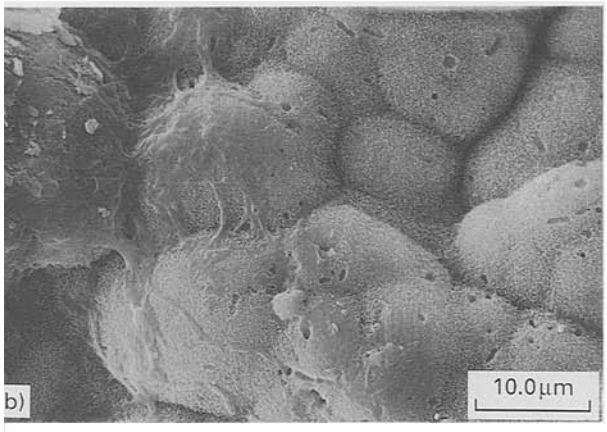

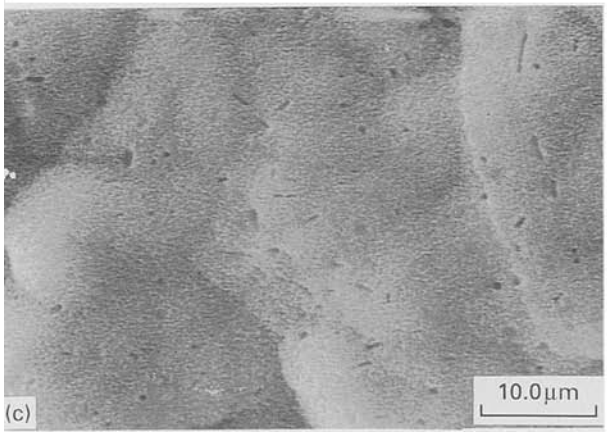

Figure 12 Large magnification of Fig. 11 for the plasma-sprayed (a) CHA, (b) SMHA, and (c) SHA coatings.

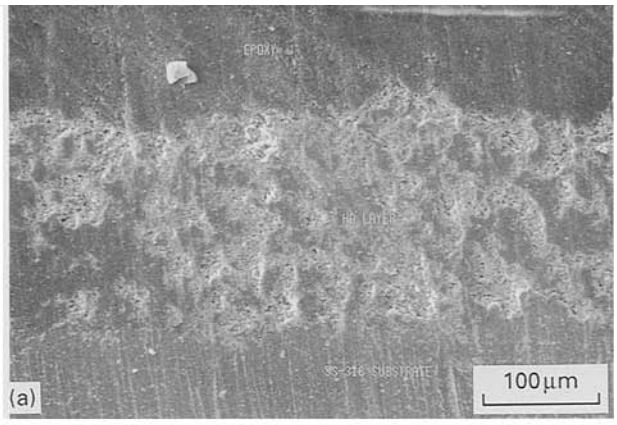

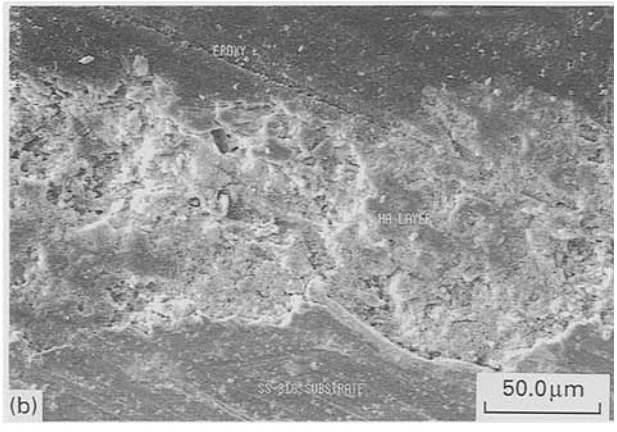

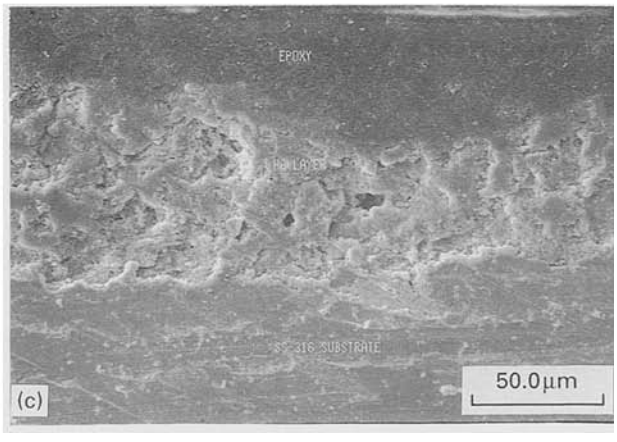

Figure 13 Cross-section observation of the plasma-sprayed (a) CHA, (b) SMHA, and (c) SHA coatings.

demonstrate a large number of holes, which resembles those found in the surface of bioactive glass material [23], and which appear to be explainable in terms of the diffusion of ions from the coating surface to the surrounding SBF.

The coating surfaces are likely to be relatively dense and homogeneous in appearance. However, from the cross-section observations, numerous pores are present in the plasma-sprayed SHA coating (Fig. 13c) compared with those of using the CHA and SMHA powders (Fig. 13a and 13b, respectively). The bonding strength between the coatings and substrate is thus low for SHA (i.e. 30 MPa) compared to CHA (45 MPa) and SMHA (37 MPa). The SMHA coating showed less particle packing density than that the CHA coating; however, more details of bonding properties and subsequent *in-vivo* evaluation will be reported elsewhere.

4. Conclusions

A chemically stable and satisfactory HA coating can be achieved using synthesized, small-sized crystalline hydroxyapatite powder having a short-range-order apatitic structure, with stoichiometric ratio of 1.67. Although the bonding strength is lower than that when using the commercial hydroxyapatite powder, a crack-free surface with SMHA does provide a promising feature, both biochemically and mechanically. The SHA powder gives rise to a crack-free coating, however, the existence of an impurity phase induced by plasma spraying restricts its potentiality for clinical applications.

Acknowledgements

The authors are grateful for financial support from the

Ministry of Economic Administration, ROC, towards this research.

References

1. K. DE GROOT, R. GEESINK, C. P. A. T. FLEIN and P. SEREKIAN, *J. Biomed. Mater. Res.* **21** (1987) 375.
2. G. A. VAN BLITTERSWIJK, J. J. GROTE, W. KUIJPERS, W. TH. DAEMS and K. DE GROOT, *Biomaterials* **7** (1986) 137.
3. H. A. HOOGENDOORM, W. RENOOIJ, L. M. A. AFFERMANS, W. VISSER and P. WITTEBOL, *Clin. Orthop.* **187** (1984) 281.
4. S. D. COOK, K. A. THOMAS, J. F. KAY and M. JARCHO, *ibid.* **230** (1988) 303.
5. R. G. T. GEESINK, K. DE GROOT and C. P. A. KLEIN, *J. Bone Joint Surg.* **70B** (1988) 17.
6. D. P. RIVERO, J. FOX, A. K. SKIPOR, R. M. URBAN and O. J. GALANTE, *ibid.* **22** (1988) 191.
7. L. G. ELLIES, D. G. A. NELSON and J. B. D. FEATHERSTONE, *Biomaterials* **13** (1983) 313.
8. W. R. LACEFIELD, "Hydroxyapatite coating in bioceramics", edited by P. Ducheyne and J. Lemons, *Ann. N. Y. Acad. Sci.* **523** (1988) 72.
9. J. F. OSBORN, in "Bioceramics", Vol. 1, edited by H. Oonishi, H. Aoki and K. Sawaki (Ishiyaku Euro America, Kyoto, Japan, 1989) p. 388.
10. H. OONISHI, M. YAMAMOTO, H. ISHIMARU, E. TSUJI, S. KUSHITANI, M. AONO and Y. UKON, in "Bioceramics", Vol. 1, edited by H. Oonishi, H. Aoki and K. Sawaki (Ishiyaku Euro America, Kyoto, Japan 1989) p. 400.
11. S. R. RADIN and P. DUCHEYNE, *J. Mater. Sci. Mater. Med.* **3** (1992) 33.
12. D. P. RIVERO, J. FOX, A. K. SKIPOR, R. M. URBAN and J. O. GALANTE, *J. Biomed. Mater. Res.* **22** (1988) 191.
13. L. G. ELLIES, D. G. A. NELSON and J. B. D. FEATHERSTONE, *Biomaterials*, **13** (1992) 313.
14. H. OGUCHI, K. LSHIKAWA, S. OJIMA, Y. HIRAYAMA, K. SETO and G. EGUCHI, *ibid.* **13** (1992) 471.
15. D. M. LIU and H. M. CHOU, unpublished work.
16. B. O. FOWLER, *J. Inorgan. Chem.* **13** (1974) 194.
17. W. VAN RAEMDONCK, P. DUCHEYNE and P. DE MEESTER, in "Metal and Ceramic Biomaterials", Vol. 2, edited by P. Ducheyne and W. Hasting (CRC press, Boca Raton, FL. 1984) p. 149.
18. J. G. C. WOLKE, J. M. A. DE BLIECK-HOGERVORST, W. J. A. DHERT, C. P. A. T. KLEIN and K. DE GROOT, *J. Therm. Spray Technol.* **1** (1992) 75.
19. K. DE GROOT, *Biomaterials* **1** (1980) 47.
20. C. P. A. T. KLEIN, A. A. DRIESSEN, K. DE GROOT and A. VA DEN HOOFF, *J. Biomed. Mater. Res.* **17** (1983) 769.
21. H. C. W. SKINNER, J. S. KITTLRBERGEN and R. A. BEELE, *J. Phys. Chem.* **79** (1975) 2017.
22. H. NEWESELY, *J. Oral. Rehab.* **4** (1977) 97.
23. D. M. LIU and F. J. SHIEH, submitted to the Journal of Non-Crystalline Solids.
24. T. KOKUBO, *J. Non-Cryst. Solids* **120** (1990) 138.

Received 6 January
and accepted 14 September 1993